CHALMERS
UNIVERSITY OF TECHNOLOGY

Zero-Offset Frequency Locking of Lasers At Low Optical Powers With an Optical Phase Locked Loop

Citation for the original published paper (version of record):
Larsson, R., Vijayan, K., Andrekson, P. (2024). Zero-Offset Frequency Locking of Lasers At Low Optical Powers With an Optical Phase Locked Loop. Journal of Lightwave Technology, 42(3): 1183-1190. http://dx.doi.org/10.1109/JLT.2023.3330707

(article starts on next page)

Zero-Offset Frequency Locking of Lasers at Low Optical Powers with an Optical Phase Locked Loop

Rasmus Larsson, *Student Member, IEEE*, Kovendhan Vijayan, *Member, IEEE* and Peter A. Andrekson, *Senior Member, IEEE*

***Abstract*—Frequency locking of lasers is fundamental to a vast number of applications within the field of optics. Usually, when locking a laser to an optical reference wave, it is imperative that locking can be maintained in spite of low reference powers. Previous solutions to frequency locking involve injection locking and/or optical phase locked loops. While previous works have shown locking to weak waves, we extend the lowest demonstrated optical power locked to by approximately 20 dB, realizing locking down to -90 dBm, using a novel digital dither optical phase-locked loop. Measurements of the locked laser phase error verify the performance. The loop design circumvents the presence of a dither on the locked laser light, hence avoiding dither penalties, and low-power locking is realized via coherent detection gain without any optical amplifiers. Low phase noise standard deviations of less than 20°at -80 dBm optical power and Allan deviation of $3 \cdot 10^{-16}$ at 1s averaging time indicate great potential for a variety of applications within optical sensing, communications, and metrology.**

***Index Terms*—Laser frequency locking, Optical phase-locked loop, Low power, phase noise, sensing, communications, metrology.**

I. Introduction

FREQUENCY and phase locking of optical waves is fundamental to many applications within optical metrology, sensing, and communications. It can enhance individual frequency comb lines, useful for laser spectroscopy [1] or time transfer [2]. In optical coherent detection, frequency and phase locking of the local oscillator (LO) can suppress phase noise in the digital carrier recovery [3] and allows phase to be measured in real-time. Homodyne optical frequency locking of lasers further enables pump carrier regeneration in phase-sensitively pre-amplified receivers [4] and coherent combining of laser light in free-space laser applications [5].

In many cases, the optical wave one wishes to lock to may be of low optical power due to significant optical losses, such as in vast fiber networks, free space channels or, for instance, in power inefficient frequency comb generation. For these applications, it is crucial that locking can be achieved despite the resulting low power of the reference wave. Although Doppler shifts and added phase noise from transmission media affect the locking, the individual lasers' non-deterministic phase noise and frequency drift usually pose the main challenge.

This work was supported by the Swedish Research Council (VR) under grant VR-2015-00535. (*Corresponding author: Rasmus Larsson*)

Rasmus Larsson and Peter A. Andrekson are with the Photonics Laboratory, Department of Microtechnology and Nanoscience, Chalmers University of Technology, Gothenburg 41296, Sweden (e-mail: rasmus.larsson@chalmers.se; peter.andrekson@chalmers.se).

Kovendhan Vijayan was with the Photonics Laboratory, Department of Microtechnology and Nanoscience, Chalmers University of Technology, Gothenburg 41296, Sweden. He is now with the Nokia Bell Labs, 600 Mountain Ave, Murray Hill, NJ 07974, USA (e-mail: kovendhan.vijayan@nokia-bell-labs.com).

Currently, optical frequency locking is most often achieved using optical injection locking (OIL) [6] and optical phase-locked loops (OPLLs) [7], either individually or combined. In OIL, a continuous wave seed light is injected into a slave laser, which adopts the seed frequency with a phase proportional to the slave laser and seed frequency offset. The ratio between injected and ejected power of the slave laser determines the allowable offset frequency for maintained locking. In contrast, most OPLLs lock at a frequency offset [7]. Here, the beat note between a reference carrier wave (REF) and a local oscillator wave (LO) from a slave laser serves as the error signal for a control system controlling the slave laser frequency.

Locking at low powers has been demonstrated using both OIL and OPLLs. For instance, a dither-based OPLL [8] for homodyne local oscillator locking has shown promising use for coherent reception at low signal powers in [9]. Meanwhile, in [10], locking down to -72 dBm optical power (lowest reported value) was achieved using an OIL-OPLL [11].

Here, we present a novel digital dither-OPLL for locking to a reference carrier wave and demonstrate homodyne locking of two independent lasers at -80 to -90 dBm optical powers. The OPLL impact on frequency locking is discussed and characterized in terms of various performance metrics pertaining to short-term phase noise and long-term frequency stability.

Our OPLL design has several features that promote its performance and versatility at low-power frequency locking. The locked laser light is extracted prior to dithering, allowing a stronger dither and, hence, locking at lower powers without any dither penalty. Our system further relies on coherent detection gain from the strong slave laser light for the amplification of weak reference waves. This allows implementation at a wide range of wavelengths as opposed to the erbium-doped fiber amplifier (EDFA) pre-amplified OIL-OPLL in [10]. The zero-offset locking also makes it insensitive to any instability of the dither frequency, which would otherwise affect the long-term stability of the lock, something which offset-locking OPLLs are concerned with in terms of their offset frequency synthesizer stability [12]. In contrast to OIL, our second-order, type 2, OPLL [13], does not produce a phase error from frequency offsets between the REF and the LO, thereby eliminating the transfer of frequency offsets to phase noise and limiting its effect on long-term stability. The spectral discrimination of the dither-OPLL frequency lock can also be made much smaller in comparison to OIL, e.g., enabling the distinction of tightly spaced comb lines down to the sub 100 kHz level. The locking bandwidth is further decided by the chosen OPLL loop bandwidth, which can easily be changed, rather than the injection ratio in OIL. Finally, the digital implementation allows for versatile filtering and processing of the error signal, which could improve system performance.

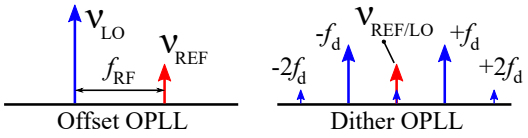

Fig. 1. Spectral domain depiction of frequency offset-locking and phase dither-locking.

Parts of this work were presented in [14], where the operation of our dither-OPLL was verified for pump carrier regeneration in a phase-sensitively amplified receiver at -83 dBm power. Here, we focus on the OPLL and expand upon the previous demonstration by further describing the working principle of the dither OPLL and relevant performance metrics. Additional results are presented in terms of coherence functions, Allan deviations, and phase slips. We further include and compare with numerical simulations of phase error standard deviation as well as Allan deviation and noise-induced phase slips. Further discussion and ultimate limits are also included.

II. The Dither-Optical Phase Locked Loop

The key difference between a dither-OPLL and a frequency-offset OPLL is the use of a phase dither (sinusoidal phase modulation) on the LO rather than a fixed frequency offset to create the error signal. The locking process of both the offset and dither OPLL is illustrated in Fig. 1. In a frequency offset-OPLL, the beat note obtained on a photodetector (PD) from interference between the REF and LO, is demodulated using a radio frequency (RF) oscillator at the offset frequency f_{RF}. This generates a baseband signal containing information of the phase error. In a dither-OPLL, when a dither is applied, the spectral line of the LO is redistributed at multiples of the dither frequency f_d. When these lines beat with the REF at the PD, the same baseband phase error information is obtained after demodulation at the dither frequency. Note that the inherent zero-offset frequency lock of the dither-OPLL makes it insensitive to any variations in f_d. In contrast, any fluctuation in f_{RF} would result in a frequency variation of the locking in an offset-OPLL w.r.t. the REF. It is moreover required that f_d, as with f_{RF} in an offset-OPLL, is chosen much larger than the spectral content of phase and frequency variations between the LO and REF to be compensated.

To phase-lock the LO to the REF, the OPLL must actively control the LO frequency and phase to minimize the phase error. Our OPLL design, presented in Fig. 2, achieves this via current control of the local (slave) laser and an electro-optic phase modulator (ϕ_c-mod) on the laser output for frequency and phase control of the LO, respectively. Incorporating ϕ_c-mod provides an extra parameter of control and has previously been shown to extend the OPLL bandwidth [9]. After frequency and phase control, the LO is locked to the REF.

A splitter is used to obtain a part of the LO light, which is sent through a secondary electro-optic phase modulator (ϕ_d-mod) that adds a phase dither $\phi_d \cos(2\pi f_d t)$ of magnitude ϕ_d to create the error signal. Introducing the dither in a separate phase modulator after extracting the useful locked LO eliminates the effect of spurious tones and phase error penalty from the dithering. This allows increasing the dither magnitude

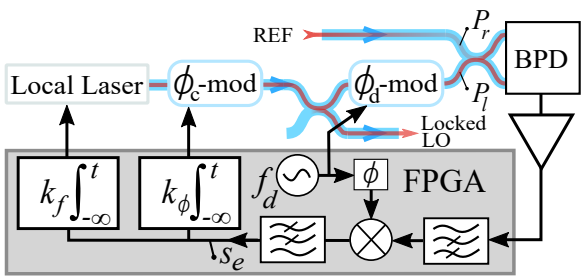

Fig. 2. A schematic of the dither-OPLL laser locking setup. The LO light is dithered in ϕ_d-mod and interfered with the REF at the BPD. The detected signal is amplified, sampled by the FPGA, then high-pass filtered and mixed with a synchronized copy of the dither into a baseband error signal. The low-pass filtered error signal then drives two integrators for phase and frequency control in ϕ_c-mod and via current control in the local laser, respectively.

to maximize the f_d-beat note and the resulting OPLL signal-to-noise ratio (SNR), enabling improved locking performance at lower REF powers.

The dithered LO of power P_l interferes with the weak REF light of power P_r in a 50/50-coupler. A balanced photodetector (BPD) is used to detect the beat note, which helps to reduce the transfer of intensity noise from the comparatively strong LO to the error signal. The BPD signal is subsequently amplified in a low noise amplifier (LNA) of 1 MHz bandwidth before sampling, filtering, and demodulation at f_d in a Red Pitaya field-programmable gate array [15] with a 125MS/s, 14-bit analog to digital converter. The choice of dither frequency in this work, $f_d = 1$ MHz, was limited by this LNA bandwidth.

The generated baseband error signal s_e after demodulation is proportional to $2J_1(\phi_d)\sqrt{P_l P_r}\sin\phi_e$ where $J_1(x)$ is the Bessel function of the first kind and ϕ_e is the residual phase error between LO and REF after locking. A ϕ_d equal to 0.59π rad then maximizes the power of s_e and the OPLL SNR. However, due to the limited voltage supply to ϕ_d-mod, the maximum ϕ_d in this work was limited to 0.27π rad.

For small ϕ_e, the error signal is proportional to the phase error ($s_e \propto \phi_e$), and a linear second-order OPLL of type 2 is achieved as s_e is fed to two separate integrators with equivalent total loop gains k_f and k_ϕ for the frequency and phase control, respectively. The choice of loop gains further determines the OPLL bandwidth, typically several tens of kHz in this work, which provides a much narrower frequency discrimination than the often > 1 MHz locking ranges in OIL systems.

It should be noted that when using only one BPD, the dither-OPLL with $\phi_d = 0.59\pi$ has a fundamental SNR advantage of a factor $4J_1(0.59\pi)^2 \approx 1.35$ (2 if all LO power was modulated onto the $\pm 1 f_d$-tones) compared to an offset-OPLL, as the error signal of a dither-OPLL is contained in one quadrature phase only in contrast to the offset-OPLL beat tone. Also, as adding a phase modulator (ϕ_d-mod) and driving it using a synchronized copy of f_{RF} as the dither are the simple steps of converting an offset-OPLL into a dither-OPLL, conversion between the two types is straightforward by using commercial components.

A. Residual phase error

In the ideal case, the LO should adopt the exact frequency and phase characteristics of the REF via locking in the OPLL.

Although the dither-OPLL design minimizes ϕ_e, it will exhibit a non-zero value that fluctuates with time. It is, therefore, of interest to understand the residual phase error in terms of its time and frequency characteristics to evaluate the quality of the locked LO w.r.t. the REF and the performance of the OPLL. While we will cover these aspects in later sections, we here focus on the phase error variance $\sigma^2_{\phi_e}$, which provides an important quality metric of the OPLL as well as the metric of minimization when optimizing the OPLL parameters.

There are two main contributions to the residual phase error. One is the uncompensated phase variations between LO and REF beyond the OPLL bandwidth $B_L = k_\phi/2\pi$ [9]. The other is the transfer of noise within the OPLL noise bandwidth $B_n = \frac{\pi}{2}\left(\frac{k_\phi}{2\pi} + \frac{k_f}{k_\phi}\right)$ [16] ($\approx k_\phi/4$, typically) from the baseband error signal to the residual phase error. Minimizing the phase noise contribution involves increasing the OPLL bandwidth, whereas minimizing the OPLL noise contribution means reducing the OPLL bandwidth. Minimizing $\sigma^2_{\phi_e}$ therefore requires optimizing the OPLL bandwidth given the external conditions: REF power P_r, the power spectral density (PSD) of the relative phase noise between LO and REF S_ϕ and the OPLL noise PSD S_n.

The exact theoretical treatment of phase error contributions is covered in the Appendix. Assuming zero loop delay, slow environmental-induced frequency drifts, Lorentzian phase noise PSD $S_\phi = 2\Delta\nu/\pi f^2$ with linewidth $\Delta\nu$ and white OPLL noise, the minimized phase error variance can be written

$$\sigma^2_{\phi_e} = \sqrt{\frac{\pi\Delta\nu S_n}{2J_1(\phi_d)^2 P_l P_r}}. \tag{1}$$

In our OPLL, $S_n = \text{NEP}^2/2$ where NEP$= 14$ pW/$\sqrt{\text{Hz}}$ is the noise equivalent power of the used BPD. The LO power was set at $P_l = -17$ dBm to avoid saturation. With improved detection, the ultimate limit is reached for a shot-noise (SN) limited system for which $S_n = h\nu P_l$ (assuming BPD quantum efficiency $\eta = 1$), where h is Planck's constant and ν is the optical frequency.

The variance in (1) provides the theoretical minimum phase error variance of the demonstrated OPLL and relates the impact of the stated external conditions on the final phase error. Of note is that halving the linewidth $\Delta\nu$ allows for halving the REF power P_r at maintained OPLL performance. A narrow laser linewidth is, therefore, essential to reach low OPLL sensitivities. Additional but smaller contributions to $\sigma^2_{\phi_e}$ for the investigated OPLL arise from its digital implementation and finite frequency resolution of the frequency control (14-bit digital to analog converter) as well as the phase error produced by frequency drifts in a second-order, type 2, OPLL.

III. Phase Error Measurements

To demonstrate and evaluate the frequency locking using the presented OPLL, the residual phase error was measured using the setup shown in Fig. 3. In addition, relative intensity noise (RIN) on the locked LO was measured to investigate any effect of the locking on the LO intensity. During all measurements, the OPLL bandwidth was optimized for the best OPLL performance. Raw data and processing code is available in [17].

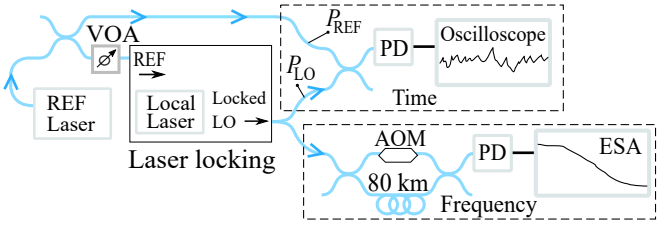

Fig. 3. Measurement setup for the residual phase error in the time and frequency domain. PD: Photodetector with 125 MHz bandwidth. AOM: Acousto-optic modulator. ESA: Electrical spectrum analyzer. $P_{\text{REF}} = P_{\text{LO}} \approx -22$ dBm. Time box: interference of REF with the Locked LO. Frequency box: Delayed self-heterodyne interferometry.

The performance of the OPLL depends on the characteristics of the LO and REF as well as the OPLL parameters. In this work, a Thorlabs distributed fiber Bragg (DFB) external cavity laser served as the local (slave) laser, acting as the LO. The REF was generated from an NKT fiber laser. Both lasers emitted at a wavelength of $\lambda = 1550.65$ nm and exhibited sub-kHz linewidths, which together sum to roughly $\Delta\nu = 350$ Hz. The REF light was separated using a splitter where one output served as a REF reference, and the other was sent to the REF input of the OPLL. Prior to interference in the 50/50-coupler of the OPLL, a variable optical attenuator (VOA) was used to sweep the REF power (P_r in Fig. 2) to investigate the locking performance at different powers. Polarization controllers were used throughout the setup to match the polarizations of all waves at all points.

A. Time domain measurement

To directly sample the residual phase error in time, the locked LO and the reference REF of equalized optical powers were interfered in a 50/50-coupler with one output detected in a PD (Time box in Fig. 3). The generated PD signal $I = I_A + I_B \sin\phi_e$ was then sampled in the Red Pitaya sampling oscilloscope and saved for offline processing where the phase error was extracted using characterized values of I_A and I_B, as $\phi_e = \sin^{-1}([I - I_A]/I_B)$. This evaluation assumes $\phi_e \in [-\frac{\pi}{2}, \frac{\pi}{2}]$ which was verified for the used measurement batches. Five batches of 16,384 points for each measured power P_r and four different time frames of 0.13 ms, 1.04 ms, 16.7 ms, and 0.13 s were captured.

B. Frequency domain measurement

The phase noise PSDs of the free-running and locked lasers were measured in an electrical spectrum analyzer (ESA) using self-heterodyne interferometry [18] with an 80 km fiber delay and a 20 MHz AOM (Frequency box in Fig. 3).

IV. Phase and Intensity Noise

For applications using coherent reception of signals, such as in sensing and communications, phase noise caused by the OPLL must be minimal and well characterized. Here, we cover the phase error in terms of its probability distributions, standard deviation, PSD, and degree of coherence.

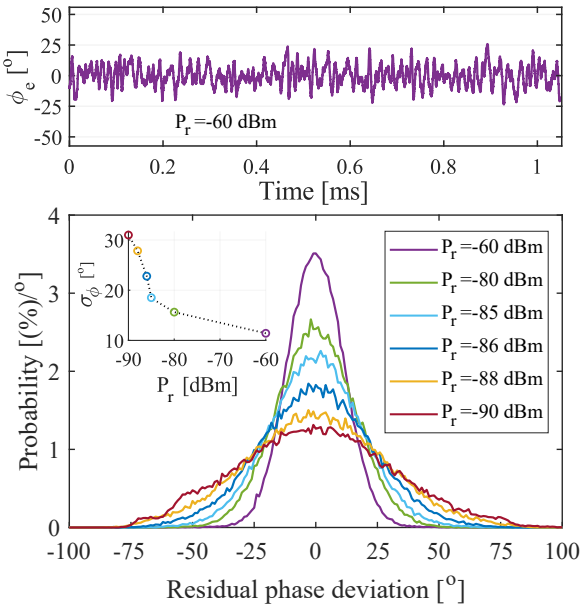

Fig. 4. Top: ϕ_e vs. time from a 1.04 ms time frame (64 ns sampling time). Bottom: The ϕ_e distribution averaged from the 16.7 ms time frame measurements (spectral content of $f \in [60\text{Hz}, 0.98\text{MHz}]$) for different REF powers P_r. The inset shows the associated phase error standard deviations.

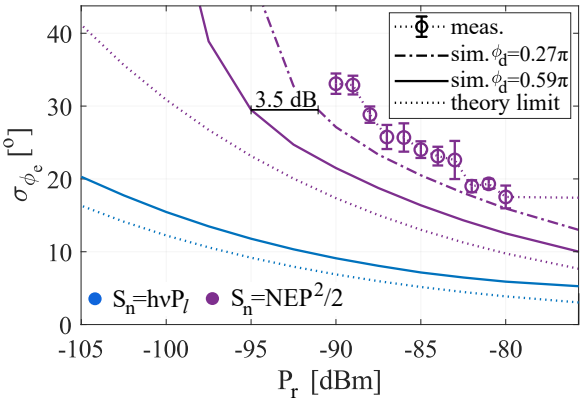

Fig. 5. σ_{ϕ_e} vs. P_r with standard deviation error bars, from the time domain measurement averaged over time frames 0.13 s and 1.04 ms. Simulated curves are also included as well as theoretical limits with $\phi_d = 0.59\pi$ for both $S_n = \text{NEP}^2/2$ and $S_n = 2h\nu P_l$ based on (1).

The time domain characteristic of the residual phase error was obtained via the time domain measurement and is presented in Fig. 4. The Top shows a typical phase error time variation at $P_r = -60$ dBm. The phase error probability densities in the Bottom demonstrate the normal distribution of ϕ_e and how the corresponding standard deviation increases with a decrease in the REF power, similar to (1).

Phase error standard deviations over a broader spectral content ($f \in [7.5\text{Hz}, 15\text{MHz}]$) are presented in Fig. 5 (averaged from time frames 0.13 s and 1.04 ms). Numerical simulations of optimum σ_{ϕ_e} are also presented as well as theoretical curves based on (1). Simulations incorporate the loop delay of the OPLL (characterized to be ≈ 2 μs), see the Appendix.

Comparison of measurement and simulation (purple dash-dot) in Fig. 5 indicates good OPLL optimization at the investigated P_r with only a few dB of difference in P_r, coming from system implementation penalties. The 3.5 dB difference between the $\phi_d = 0.27\pi$ and $\phi_d = 0.59\pi$ cases further emphasizes a potential sensitivity improvement of the OPLL for an optimized value of ϕ_d. The difference between the solid lines and dotted lines further emphasizes the degrading OPLL performance due to the loop delay. The blue vs. purple curve comparison indicates a potential improvement of OPLL performance when the ultimate shot noise limit is reached. A potential 25 dB sensitivity improvement is observed at $\sigma_{\phi_e} = 17^o$ between measurement and the SN-limited theory.

To quantify the benefit of separating dither and control signals, σ_{ϕ_e} was also measured with phase dithering in ϕ_c-mod. A 1.73 times larger σ_{ϕ_e} at $P_r = -80$ dBm was obtained, which shows the advantage of phase dithering (in ϕ_d-mod) after extraction of the locked LO in our design.

Fig. 4 and 5 demonstrate locking down to -90 dBm optical powers. At $P_r = -83$ dBm, the locking performance for pump carrier regeneration in a phase-sensitively pre-amplified receiver resulted in a 0.2 dB sensitivity penalty, as demonstrated in [14]. Below -90 dBm, the system experienced increased instability due to significant phase errors, and locking was challenging to maintain.

The frequency domain characteristics of the locked and free-running lasers were obtained via the frequency domain measurements and are presented in Fig. 6 a) in terms of phase noise PSDs at two different P_r. We note that the locked LO adopts the phase noise of the REF up to a frequency of 38 kHz, indicating a limited phase compensating (loop) bandwidth of the OPLL. Below this frequency, the phase noise with lower P_r is higher. This agrees with the increased σ_{ϕ_e} for lower P_r in Fig. 4, Fig. 5 and in (1). Beyond 38 kHz, the locking system adds phase noise until about 1 MHz, corresponding to the bandwidth of the control signals. The increase in phase noise above 100 kHz for P_r = -80 dBm is due to 2π phase slips in ϕ_c-mod as the driving voltage limit was reached. The occurrence of phase slips scales with k_ϕ/k_f, which was larger for P_r = -80 dBm in Fig. 6 a). These ($\approx$ 1 µs duration) phase slips are discussed further in the next section. However, slips can be circumvented either by using an additional phase modulator as in [19] or by exchanging ϕ_c-mod for proportional control of the LO frequency directly (assuming high enough LO frequency modulation bandwidth). These slips, hence, do not pose a fundamental limitation to the locking.

At smaller laser linewidths, transmission media-induced phase variations may become non-negligible. Atmospheric turbulence, for instance, may add significant phase noise, albeit typically contained within a 1 kHz ($\ll$ 38 kHz) bandwidth [20]. For weak signals, phase noise from fiber propagation is typically negligible unless for exceptionally long links [21].

Another important characteristic is the coherence of the LO, which is used in self-referenced interferometric measurement applications like optical tomography. From the phase noise PSDs in Fig. 6 a), the corresponding normalized degree of coherence $|g|$ (optical field auto-correlation) was calculated to investigate the OPLL impact on the locked LO coherence. These were normalized using the auto-correlations of the time domain measurements of ϕ_e and are presented in Fig. 6 b). Here, the locked LO is observed to inherit the coherence

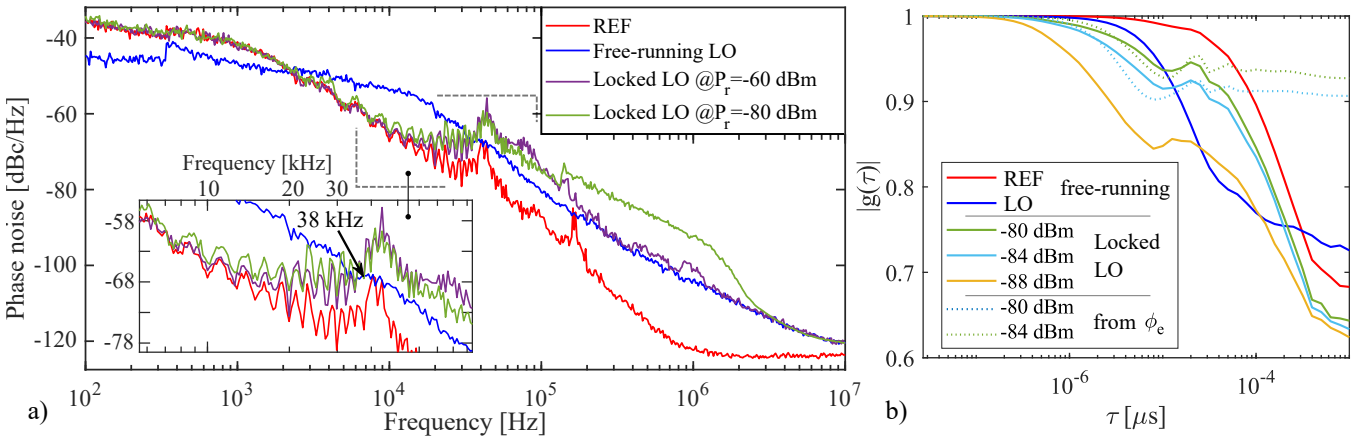

Fig. 6. a) Measured phase noise PSDs. b) The degree of coherence vs. delay τ, calculated from the PSDs in a) and normalized using time domain data.

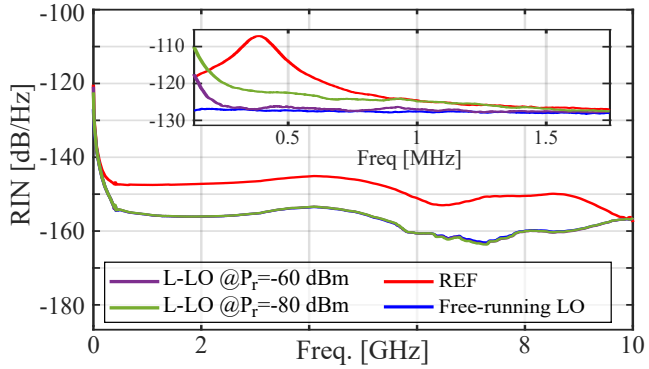

Fig. 7. RIN spectrum. At $\geq$ 2 MHz frequency, all curves except REF lie on top of each other. L-LO is Locked LO.

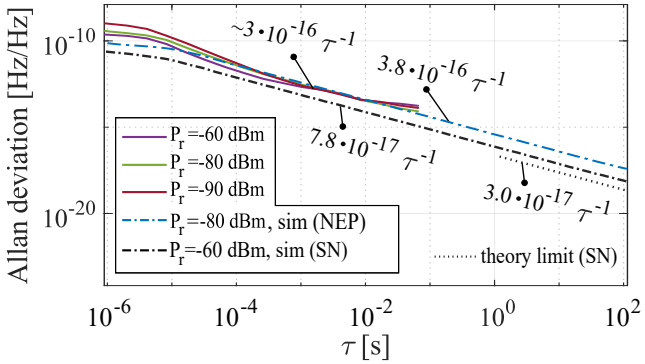

Fig. 8. Measured, simulated ($\phi_d = 0.27\pi$ at -80 dBm, $\phi_d = 0.59\pi$ at -60 dBm), and theoretical ($\phi_d = 0.59\pi$, P_r= -60 dBm) Allan deviations vs. measurement averaging time τ. NEP: $S_n = \text{NEP}^2/2$. SN: $S_n = h\nu P_l$.

characteristics of the REF for delays $\tau \gtrsim 10$ μs. The dotted lines show the pure phase error coherence as would be obtained from the locked LO and a perfect REF coherence $|g(\tau)| = 1$. As such, the dotted lines represent the impact of the OPLL on the coherence. As can be seen for decreasing P_r, the locked LO's coherence is degraded, reflecting the degrading OPLL performance for lower P_r.

For certain applications, it is of interest to know the effect of the OPLL on the intensity. The RIN spectrum of the locked LO was measured by directly detecting the locked laser on a 10 GHz bandwidth PD and is compared to that of the free-running case in Fig. 7 at the same P_r as in Fig. 6 a). Above a few MHz, the RIN of the locked and free-running LO are identical. At frequencies within the control signal bandwidth ($<$ 1MHz), we note a P_r-dependent RIN-degradation due to the locking system. However, the impact of this RIN-degradation on the various phase error measurements is negligible, as it will be for most other phase-sensitive systems.

V. Long-term stability

For metrology applications, such as spectroscopy and time transfer, the long-term stability of the laser frequency is of importance. The locking performance over time is also vital for a continuously operating communication link. Here we discuss the long-term stability between locked LO and REF in terms of Allan deviation of the fractional frequency stability. We also discuss the presence of phase slips, both due to the limited voltage supply to ϕ_c-mod and slips caused by OPLL noise.

A. Allan deviation

Locking was generally maintained for several minutes, during which the measurements were conducted. It was also observed that the lock was maintained when the relative frequency of the free-running LO and REF were kept within the frequency tracking range of the OPLL (which was ensured by manually tuning the LO current control). Although no long-term tests were made, stable locking for more than 1 hour was observed for powers down to -80 dBm. All measurements were performed in a lab environment at room temperature.

The Allan deviation was calculated from the time domain measurements and is presented in Fig. 8 for three different P_r at averaging times up to about 0.1 s. Simulated Allan deviations are included to compare and extrapolate measurements for longer averaging times. A theoretical Allan deviation limit $\sigma_\tau = \sqrt{3}\sigma_{\phi_e}/2\pi\nu\tau$ [16], with σ_{ϕ_e} based on (1) for the shot-noise limited case and $P_r = -60$ dBm, is also presented.

The measured curves reach a minimum slope of $\sim 3 \cdot 10^{-16}\tau^{-1}$, roughly ten times larger compared to the theoretical limit (at $P_r = -60$ dBm) as well as the reported measured values in [22] for an OIL-OPLL at $P_r = -41$ dBm. Closer to 0.1 s averaging time, an increase in Allan deviation is observed

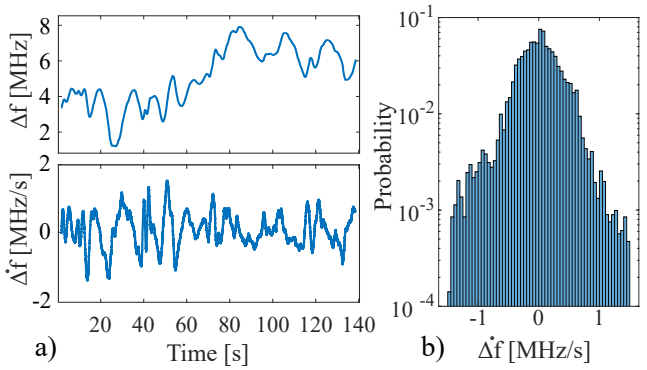

Fig. 9. a) A typical relative frequency drift between the LO and REF. b) The probability density of the drift $\Delta\dot{f}$ in a).

due to the phase instability of the used interferometer, limiting the use of any longer measurement times. Before this limit, we observe good agreement with simulations (specifically at $P_r = -80$ dBm with $S_n = \text{NEP}^2/2$), which extend beyond 0.1 s averaging time and provides a promising indication of excellent long-term frequency stability of the OPLL.

For OPLL compensation of phase noise only, the Allan deviation remains at a τ^{-1} slope. Laser frequency drift, however, translates to phase noise on the locked LO by the OPLL (being of second order and type two). Simulations under the same conditions as in Fig. 8 indicated a transition into an Allan deviation slope $\propto \tau^{-1/2}$ only above 10^3 s averaging time for a constant drift of 1.5 MHz/s. The value 1.5 MHz/s is based on the maximum frequency drift recorded between the free-running lasers used in this work, see Fig. 9 a) and b).

By increasing the frequency control gain, the effects of drift can be mitigated with negligible impact on OPLL performance, as long as the k_f-term in B_n remains negligible. The effect of drift and other higher-order time derivatives of the phase between REF and LO may also be reduced by increasing the order of the OPLL, something which is made simpler thanks to its digital implementation. At much longer averaging times, other effects not considered here, such as aging electronics, may also impact long-term stability.

B. Phase slips

Phase slips in the OPLL consist of short periods where the phase error transitions from zero mean to a mean of 2π, which acts as a neighboring and repeating operating point of the loop. During the transition, the OPLL is momentarily out of lock, which can have adverse effects depending on the application. In communications, this would result in a large error burst.

Phase slips in the OPLL occur whenever the voltage limit to ϕ_c-mod is reached, when the OPLL is programmed to perform a voltage step back, i.e., a 2π phase-jump. A phase error time measurement containing such phase slips is shown in Fig. 10 a). The 1 MHz bandwidth of the phase control signal limited the 2π transition time to 1 μs, and slips were observed to occur with close to 1kHz rates for the OPLL parameters used. As previously mentioned, these phase slips can eliminated by the implementation of a boundless phase control [19] or by adding proportional frequency control of the LO.

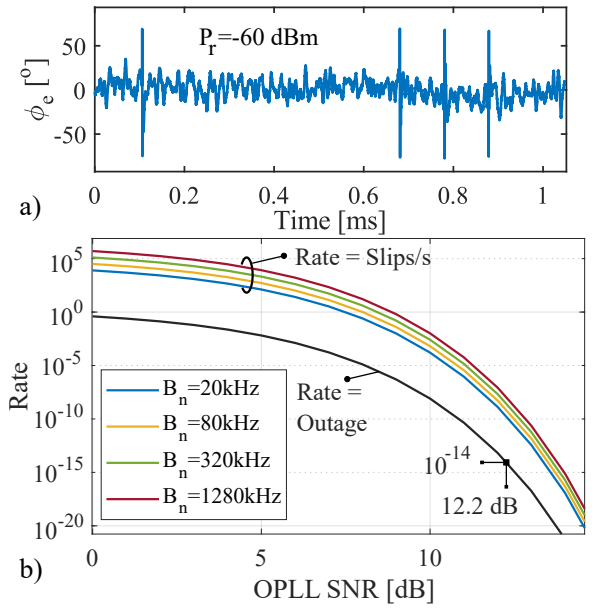

Fig. 10. a) ϕ_e vs. time from a 1.04 ms time frame measurement (64 ns sampling time) with visible 2π phase slips due to the limited ϕ_c-mod voltage supply. b) The OPLL slips/s rate due to noise for different B_n as well as the corresponding outage rate, which is independent of B_n, vs. OPLL SNR.

A second cause of phase slips is noise in the control system and is inherent to any phase-locking system, affecting all OIL and OPLL implementations. Given enough time, the noise in a control system will eventually push the phase error close enough to a $\pm 2\pi$ loop operating point for a transition to take place. The expected time for a slip to occur T_{slip} in an OPLL is described in [16] based on the OPLL SNR and noise bandwidth. Based on this, we present in Fig. 10 b) the expected number of slips per second at different OPLL SNRs ($\text{SNR}_{\text{OPLL}} = 4J_1(\phi_d)^2 P_r P_l / S_n B_n$) and noise bandwidths $B_n (\approx 1.6 B_L)$ as well as the outage rate t_{slip}/T_{slip} where $t_{slip} \approx 1/B_n$ [23] is the slip duration.

It can be seen from this result that noise-induced phase-slipping occurs more than once a second at low SNR (< 7 dB), whereas for larger SNR, the frequency of these slips rapidly reduces with increasing SNR. In our work, due to stability reasons, the OPLL was operated at minimum SNRs close to 10 dB where from Fig. 10 ($B_n = 80$ kHz) b) we expect more than a thousand seconds between recurring noise-induced phase slips. Although uncommon at high SNR, phase slips may cause issues, for instance, error bursts in a communication link, which cannot be averted. The minimum bit error rate (BER) of a link requiring a locked OPLL is equivalent to the outage rate, which indicates a minimum 12.2 dB OPLL SNR to achieve BER$< 10^{-14}$. For our OPLL, this corresponds to $P_r \tilde{>}$-85 dBm and a practically indefinite time without slips ($T_{slip} > 10^8$ s) according to Fig. 10. At lower SNR, redundancy measures should be taken to achieve a tolerable BER.

VI. Conclusion

We have presented a novel dither-OPLL and demonstrated frequency locking of two lasers of hundred Hz linewidths at 1 MHz/s frequency drifts and optical reference wave powers

down to -90 dBm, approximately 20 dB less than the lowest demonstrated carrier recovery using OIL [10]. The locking was verified and characterized in terms of measured phase noise PSDs, phase error standard deviations, and coherence between the locked lasers. We have demonstrated the benefit of separating the dither in the OPLL design to avoid dither penalties. Simulations verified the optimized performance of the OPLL and together with theoretical limits, we highlighted the potential improvements in OPLL performance (up to 25 dB in sensitivity) with optimal dither magnitude, loop delay and detection schemes.

A minimum Allan deviation slope versus averaging time τ was measured as $\approx 3 \cdot 10^{-16}\tau^{-1}$ at the investigated powers. This result was extrapolated to averaging times greater than 1s using simulations, which in the case of pure phase noise maintained the same slope, indicating the potential of the dither-OPLL for applications requiring long-term frequency stability. For significant frequency drifts, simulations showed degraded long-term stability, something which can be mitigated by increasing the frequency control loop gain.

To summarize, the presented dither-OPLL, which we previously verified for use in a phase sensitively pre-amplified receiver [14], exhibits no dither penalty, consists of relatively inexpensive components, and is versatile thanks to its digital implementation. It is wavelength flexible, requiring no EDFA, and may enable homodyne locking of waves at ultra-low optical powers for a wide range of applications.

ACKNOWLEDGMENTS

We would like to thank T. Wik for control theory discussions, F. Lei and C. Skehan for assistance and M. Karlsson for insightful discussions. This work was funded by the Swedish Research Council (grant VR-2015-00535).

APPENDIX
PHASE ERROR CONTRIBUTIONS

Here we provide the exact phase error variance relations. According to PLL theory, the contributions to the residual phase error variance $\sigma^2_{\phi_e}$ from phase (σ^2_ϕ) and system noise (σ^2_n) can be calculated as [16]

$$\sigma_i^2 = \int_0^\infty S_i(f)|H_i(j2\pi f)|^2 df \tag{2}$$

where index i indicates phase ϕ or noise n for the corresponding PSD S_i and OPLL transfer function H_i.

The OPLL phase and noise transfer functions are calculated from the open loop transfer function

$$K_e H_c(s) = k_\phi \frac{e^{-\tau_\phi s}}{s} + 2\pi k_f \frac{e^{-\tau_f s}}{s^2} \tag{3}$$

where $s = j2\pi f$, $K_e = 2J_1(\phi_d)\sqrt{P_l P_r}$ and τ_ϕ and τ_f are the phase and frequency control loop delays, characterized to be 2.2 μs and 1.5 μs, respectively. The phase and noise transfer functions in turn are given, respectively, as

$$H(s) = 1 + K_e H_n(s), \quad H_n(s) = -\frac{H_c(s)}{1 + K_e H_c(s)}. \tag{4}$$

Simulations in this work were based on the above relations, including stability constraints of $\pi/6$ radian phase margin of the open loop transfer function and OPLL SNR > 10 dB.

REFERENCES

[1] N. Picqué and T. W. Hänsch, "Frequency comb spectroscopy," *Nature Photonics*, vol. 13, no. 3, pp. 146–157, Mar 2019.
[2] E. D. Caldwell *et al.*, "Quantum-limited optical time transfer for future geosynchronous links," *Nature*, vol. 618, no. 7966, pp. 721–726, Jun 2023. [Online]. Available: https://doi.org/10.1038/s41586-023-06032-5
[3] E. Ip, A. P. T. Lau, D. J. F. Barros, and J. M. Kahn, "Coherent detection in optical fiber systems," *Opt. Express*, vol. 16, no. 2, pp. 753–791, Jan 2008.
[4] P. A. Andrekson and M. Karlsson, "Fiber-based phase-sensitive optical amplifiers and their applications," *Adv. Opt. Photon.*, vol. 12, no. 2, pp. 367–428, Jun 2020.
[5] Z. Chen *et al.*, "Mutual injection locking and coherent combining of three individual fiber lasers," *Optics Communications*, vol. 282, no. 1, pp. 60–63, 2009.
[6] Z. Liu and R. Slavík, "Optical injection locking: From principle to applications," *Journal of Lightwave Technology*, vol. 38, no. 1, pp. 43–59, 2020.
[7] K. Balakier, L. Ponnampalam, M. J. Fice, C. C. Renaud, and A. J. Seeds, "Integrated semiconductor laser optical phase lock loops," *IEEE Journal of Selected Topics in Quantum Electronics*, vol. 24, no. 1, pp. 1–12, 2018.
[8] F. Herzog, K. Kudielka, D. Erni, and W. Bachtold, "Optical phase locking by local oscillator phase dithering," *IEEE Journal of Quantum Electronics*, vol. 42, no. 10, pp. 973–985, 2006.
[9] M. L. Stevens, D. O. Caplan, B. Robinson, D. M. Boroson, and A. L. Kachelmyer, "Optical homodyne PSK demonstration of 1.5 photons per bit at 156 Mbps with rate-$\frac{1}{2}$ turbo coding," *Opt. Express*, vol. 16, no. 14, pp. 10 412–10 420, Jul 2008.
[10] R. Kakarla, J. Schröder, and P. A. Andrekson, "One photon-per-bit receiver using near-noiseless phase-sensitive amplification," *Light Sci. Appl.*, vol. 9, p. 153, Sep. 2020.
[11] D. S. Wu, R. Slavík, G. Marra, and D. J. Richardson, "Direct selection and amplification of individual narrowly spaced optical comb modes via injection locking: Design and characterization," *Journal of Lightwave Technology*, vol. 31, no. 14, pp. 2287–2295, 2013.
[12] M. Lipka, M. Parniak, and W. Wasilewski, "Optical frequency locked loop for long-term stabilization of broad-line DFB laser frequency difference," *Applied Physics B*, vol. 123, no. 9, p. 238, Aug 2017.
[13] P. V. Brennan, *Loop Basics*. London: Macmillan Education UK, 1996, pp. 31–57.
[14] R. Larsson, K. Vijayan, and P. A. Andrekson, "Zero-offset frequency locking of lasers at ultra-low optical powers," in *Optical Fiber Communication Conference (OFC) 2023*. Optica Publishing Group, 2023, p. Th4A.5.
[15] "RedPitaya, Swiss Army Knife For Engineers," Jun 2022. [Online]. Available: http://redpitaya.com/
[16] J. Spilker, *Digital Communications by Satellite*. Prentice-Hall, Englewood Cliffs, New Jersey, 1977, ch. 12. [Online]. Available: https://books.google.se/books?id=RkwvEAAAQBAJ
[17] R. Larsson, K. Vijayan, and P. A. Andrekson, "Data - Zero-Offset Frequency Locking of Lasers at Low Optical Powers with an Optical Phase Locked Loop," Sep. 2023. [Online]. Available: https://doi.org/10.5281/zenodo.8376587
[18] W. Ma *et al.*, "Laser frequency noise characterization by self-heterodyne with both long and short delay," *Appl. Opt.*, vol. 58, no. 13, pp. 3555–3563, May 2019.
[19] C. Madsen, "Boundless-range optical phase modulator for high-speed frequency-shift and heterodyne applications," *Journal of Lightwave Technology*, vol. 24, no. 7, pp. 2760–2767, 2006.
[20] B. P. Dix-Matthews *et al.*, "Point-to-point stabilized optical frequency transfer with active optics," *Nature Communications*, vol. 12, no. 1, p. 515, Jan 2021. [Online]. Available: https://doi.org/10.1038/s41467-020-20591-5
[21] J. Dong, J. Huang, T. Li, and L. Liu, "Observation of fundamental thermal noise in optical fibers down to infrasonic frequencies," *Applied Physics Letters*, vol. 108, no. 2, p. 021108, 01 2016. [Online]. Available: https://doi.org/10.1063/1.4939918
[22] J. Kim, D. S. Wu, G. Marra, D. J. Richardson, and R. Slavík, "Stability characterization of an optical injection phase locked loop for optical frequency transfer applications," in *2014 Conference on Lasers and Electro-Optics (CLEO) - Laser Science to Photonic Applications*, 2014, pp. 1–2.
[23] L. Palmer and S. Klein, "Phase slipping in phase-locked loop configurations that track biphase or quadriphase modulated carriers," *IEEE Transactions on Communications*, vol. 20, no. 5, pp. 984–991, 1972.